Electronic Supplementary Material (ESI) for Nanoscale.

Supplementary Information

Chemically Initiated Liquid-like Behavior and Fabrication of Periodic Wavy Cu/CuAu nanocables with Enhanced Catalytic Property

Zhiyuan Jiang,* Qiaorong Jiang, Rao Huang, Mingjun Sun, Kaili Wang, Qin Kuang, Zi-zhong Zhu* and Zhaoxiong Xie*

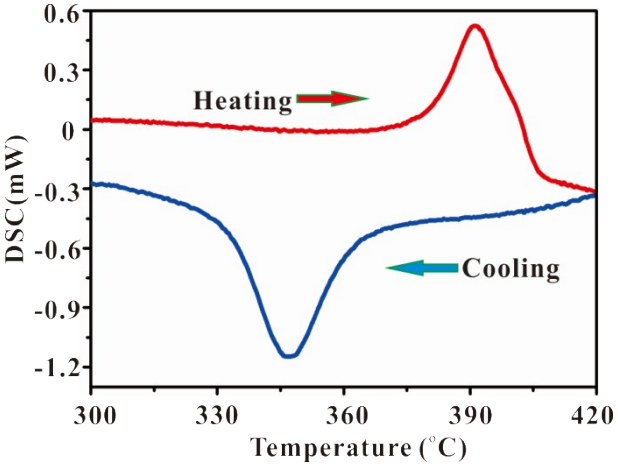

Fig. S1. DSC of straight Cu@CuAu nanocable.

Differential scanning calorimentry (DSC) was adopted to verify the melting point of Cu/CuAu nanostructure. As shown in Fig. S1, in the heating process, the curve undergoes a sharp endothermic peak around 390 °C, which can be ascribed to the melting of nanocables. While in the cooling process, the exothermic peak around 350 °C can be ascribed to the freezing of the melted CuAu alloys. Thus, it can be concluded that the melting point of Cu/CuAu nanocables is about 390 °C in the present case.

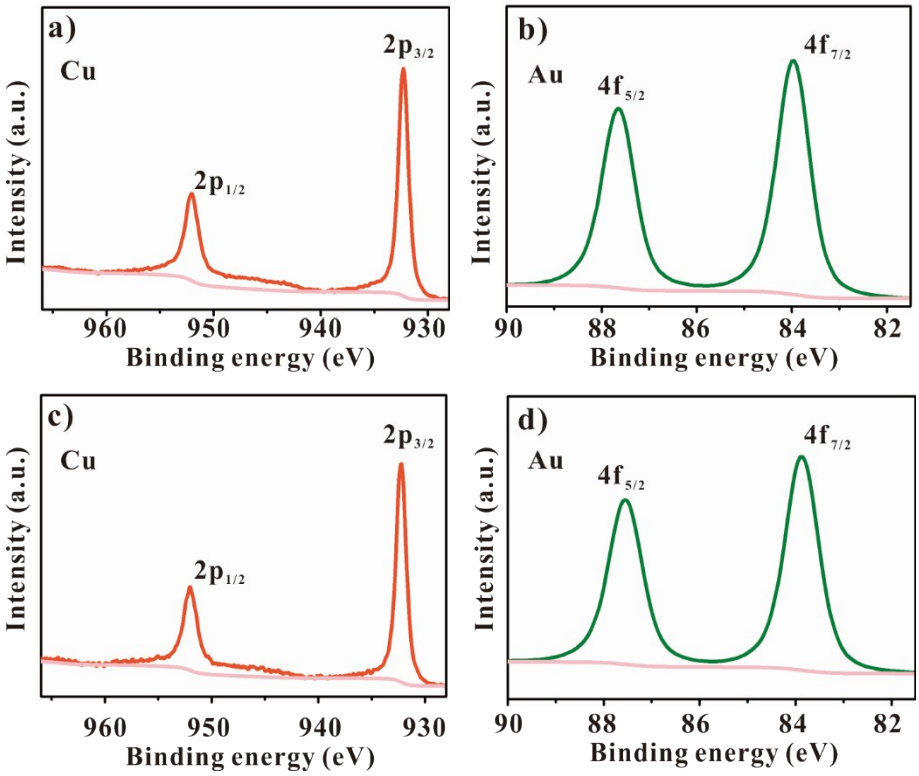

Fig. S2. XPS spectra of Cu@CuAu nanocables. a) Cu and b) Au elements of the straight Cu@CuAu nanocable; c) Cu and d) Au elements of the wavy Cu@CuAu nanocable .

XPS was employed to analyze the valance states of Cu and Au elements of the straight Cu@CuAu nanocable and the wavy one. As shown in Fig. S2, Cu 2p XPS spectrum for the CuAu alloy shows two sharp peaks with binding energies at 932.4 and 952.2 eV, corresponding well with the Cu $2p_{3/2}$ and Cu $2p_{1/2}$. And the Au 4f XPS spectrum exhibits two sharp peaks with binding energies at 83.8 and 87.4 eV, corresponding well with the Au $4f_{7/2}$ and Au $4f_{5/2}$. These results indicated the coexistence of Cu^0 and Au^0 in the shell of as-prepared nanocables. No obvious oxide states' peaks can be observed for these two samples. It can be concluded that the shell is pure CuAu alloys.

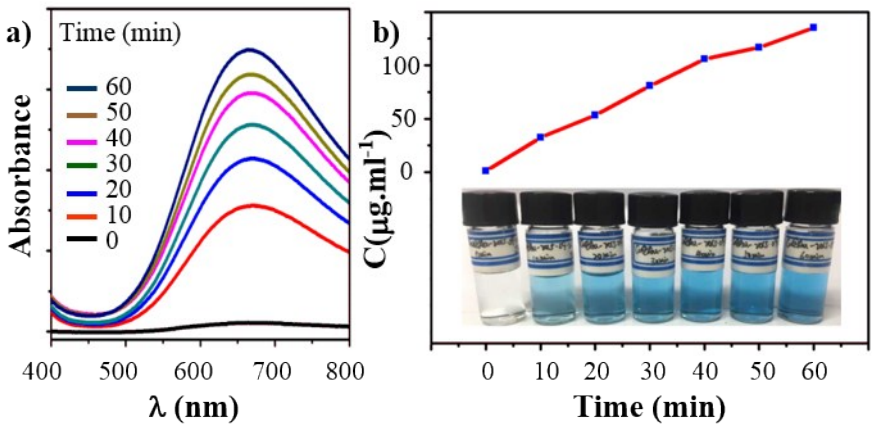

Fig. S3. Time-dependent concentration of Cu element in the supernatant of solvent treating. a) UV/Vis spectra of the supernatant, b) ICP-AES results of the supernatant. Insets of (b) are the images of the supernatant collected after different solvent treating time.

Before the solvent treating, the absorption curve of supernatant shows no obvious peaks from 400 - 800 nm (Fig. S3a). The color of the reaction solution changes to light blue after solvent treating for 10 min, and a broad peak around 650 nm appears in the absorption curve of supernatant, suggesting the formation of the Cu-amine coordination compound. With the proceeding of solvent treating, the absorption peaks further increased slowly, suggesting that Cu of the nanocable structures was continuously oxidized and dissolved into the solvent. These results could also be confirmed by the ICP-AES measurement (Fig. S3b), in which the measured concentration of Cu element in the supernatant of solvent treating increased with the lapse of time.

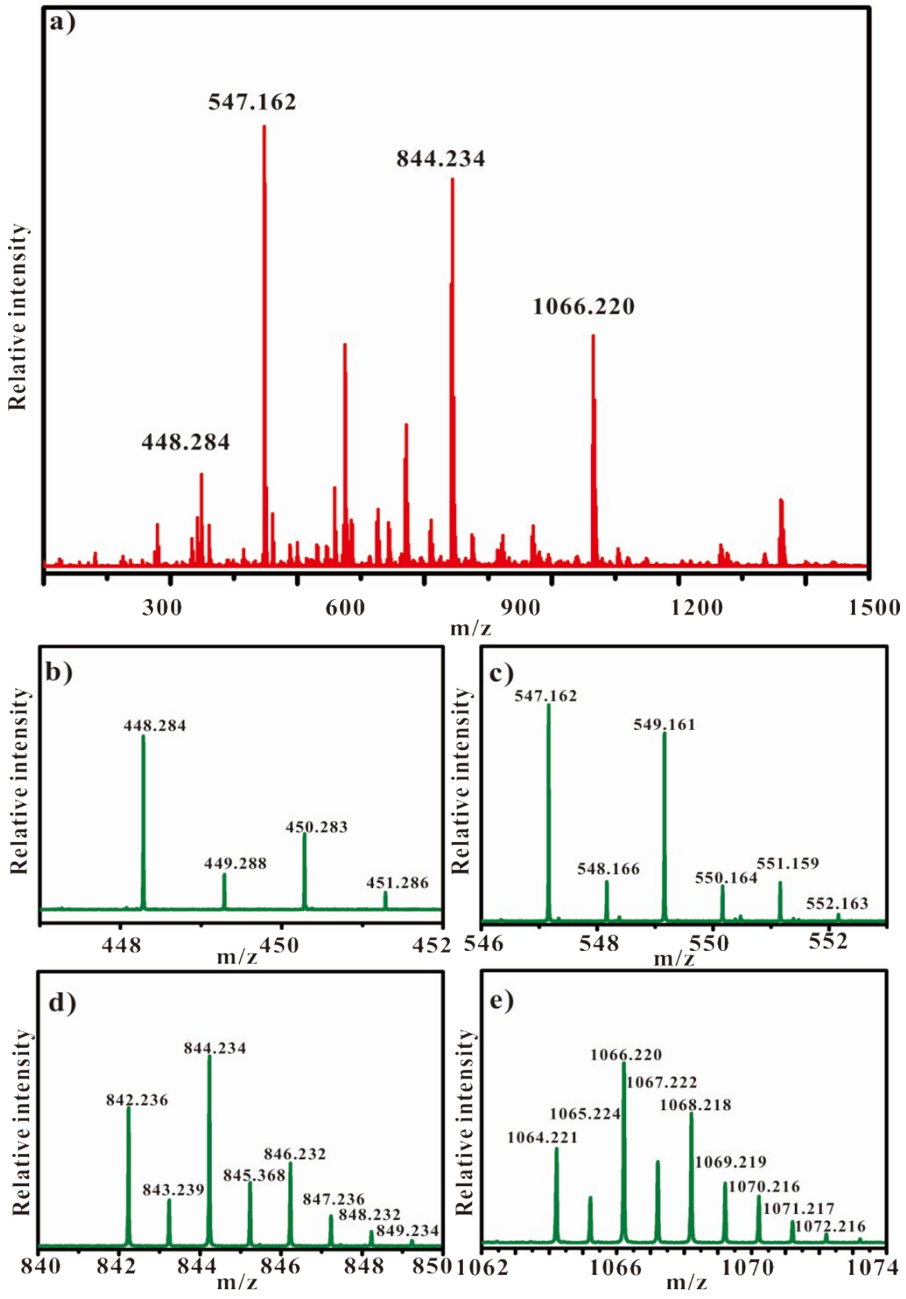

Fig. S4. Mass spectra of the supernatant solution after solvent treating using butylamine at 80 ºC for 1 h. a) MS at the m/z range from 100-1500; b), c), d) and e) are the magnified spectrums of m/z 448.284, 547.162, 844.234 and 1066.220, respectively.

The supernatant butylamine solution after solvent treating was characterized by a high-resolution electrospray ionization Fourier transform ion cyclotron resonance mass spectrometer with an electrospray ionization source in positive mode at the m/z range from 100-1500 (Fig. S4a). Intensity peaks at m/z 448.28451, m/z 449.288, m/z 450.283 and m/z 451.286 (Fig. S4b) can be obviously observed, combining the compass isotope pattern, these

characteristic isotope pattern correspond perfectly with mononuclear Cu-organic compounds. The other three prominent species at m/z=547.16250 (Fig. S4c), 844.23359 (Fig. S4d) and 1066.21958 (Fig. S4e) correspond to dinuclear, trinuclears and tetranuclears Cu-organic compounds, respectively. The definite structures of these complex still needs further deep analysis for the m/z of the corresponding species do not match simply with the stimulated m/z of $Cu_m(C_4H_{11}N)_n^{2+}$. However, it can be evidently concluded that the Cu atom on the surface of CuAu alloy can diffuse into the solvent by coordination with organic amine to form various Cu-amine complex in the presence of O_2.

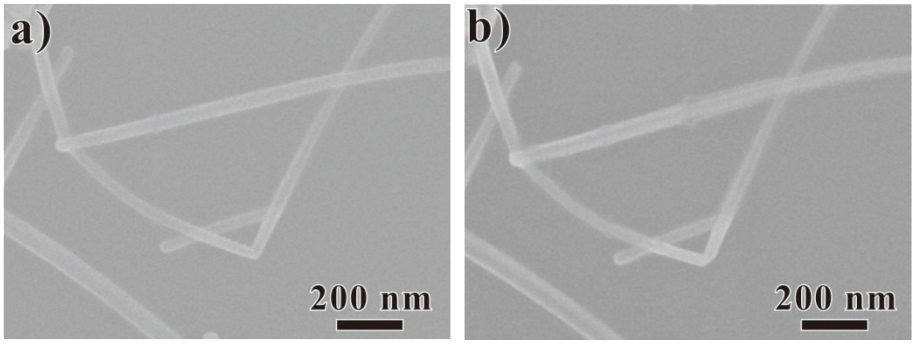

Fig. S5. The SEM images of Cu/CuAu nanocables. a) Initial image and b) the one heated at 300 °C for 1 hour without solvent and O_2.

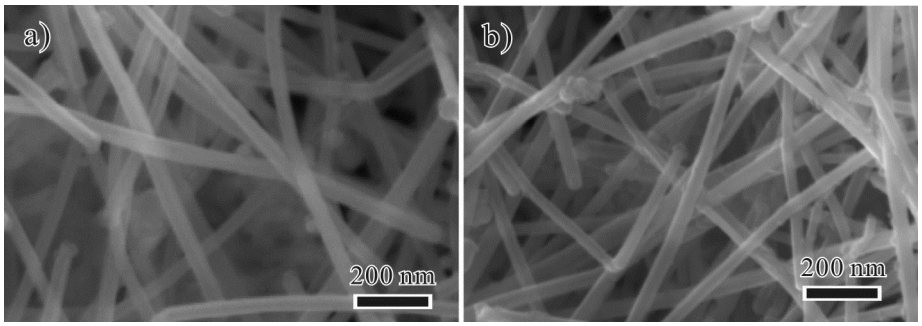

Fig. S6. Typical SEM images of the nanocables after solvent treating in 1-octadecene at 210 ºC. a) 60 min and b) 180 min.

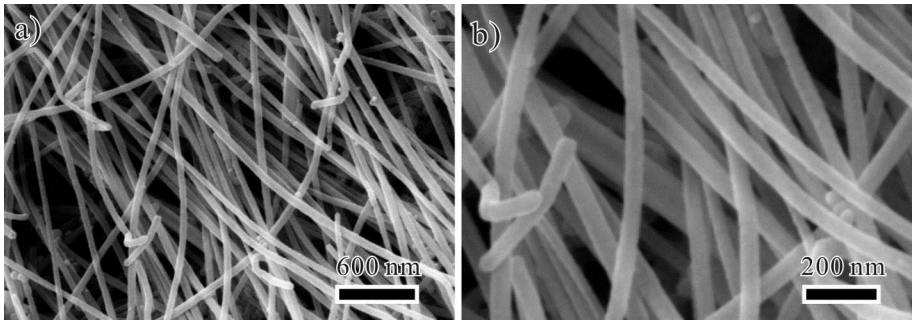

Fig. S7. Typical SEM image of the products when the solvent treating was performed under protection of nitrogen. a) Low magnification SEM image, b) enlarged SEM images.

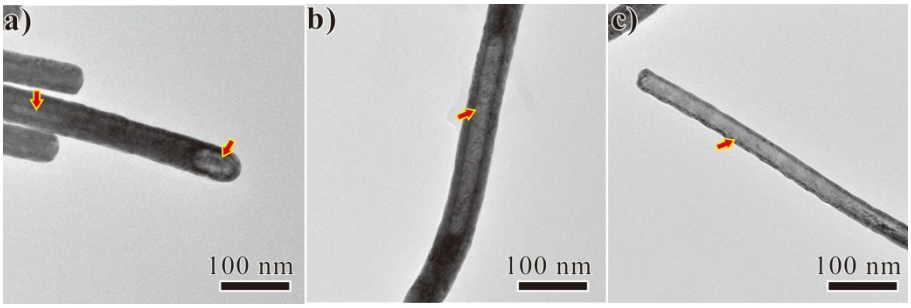

Fig. S8. TEM images of the Cu/CuAu nanocable treated at butylamine at 80 °C for a) 5 min, b) 10 min and c) 20 min.

As shown in Fig. S8a, some small and slight segmented voids (marked by arrows) sandwiched by the remaining Cu can be observed in the intermediate products treated by butylamine at 80 °C for the initial 5 min. With the increasing of the solvent treating time, obvious larger voids could be observed in the interior of Cu/CuAu nanocubles (Fig. 8b and Fig. 8c). Such evolution of the hollowing structure in the closed nanosysterm can be attributed to the uneven Kirkendall diffusion process.

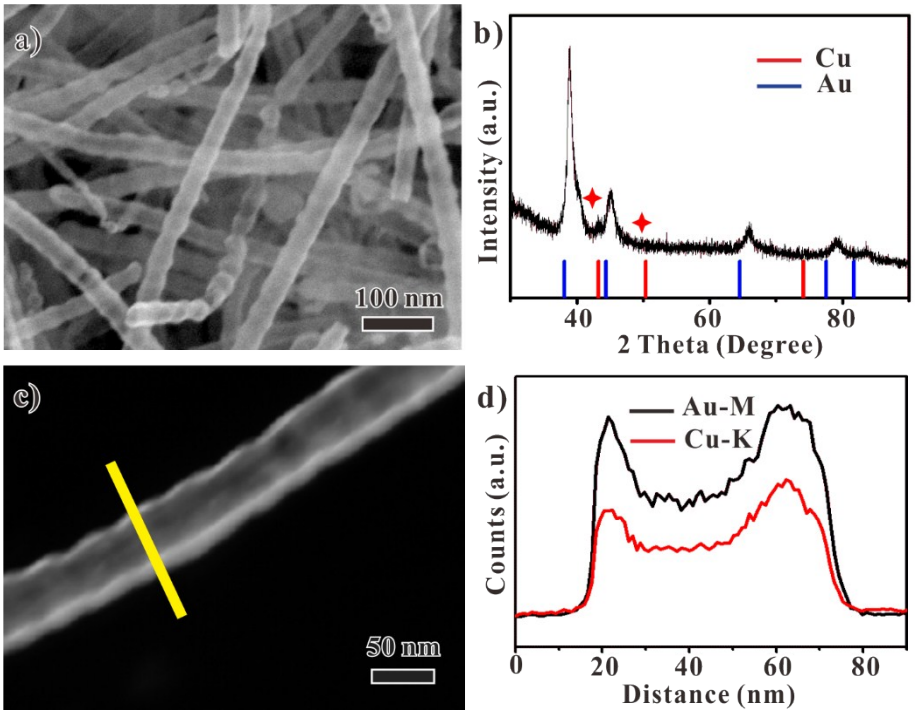

Fig. S9. Structure features of the products treated in butylamine 80 °C for 1 h. a) SEM image, b) XRD patterns, c) HAADF-STEM images and d) EDX line profiles.

The morphologiesof the products treated in butylamine 80 °C for 1 h (Fig. S9a) were almost the same as other wavy Cu@CuAu nanostructures. However, the XRD pattern (Fig. S9b) of the products was much different from that treated in n-octylamine 80 ºC for 1 hour. The main peaks could be indexed as *fcc* Cu-Au solid solution alloy structure and the peaks corresponded to the *fcc* Cu (marked by stars) could be hardly observed, which indicated that the Cu cores were almost removed in the solvent treating process. Definite compositional information was provided by high-angle annular dark-field scanning transmission electron microscopy (HAADF-STEM). It is clearly seen that the nanostructure has obvious contrast between interior and exterior from the HAADF-STEM image **(**Fig. S9c), suggesting the existence of hollow interior structure of the products. The EDX cross-sectional compositional line profiles of Au-M and Cu-K (Fig. S9d) indicate that the elements Au and Cu distribution ranges are completely overlapped and obvious enrichment in the outer layer of the nanostructure, confirming the formation of Cu-Au alloy nanotubes.

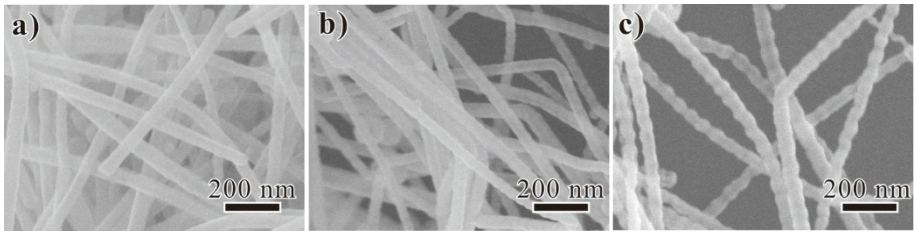

Fig. S10. SEM images of the Cu/CuAu nanocable treated by n-octylamine at 80 °C for a) 20 min, b) 40 min and c) 60 min.

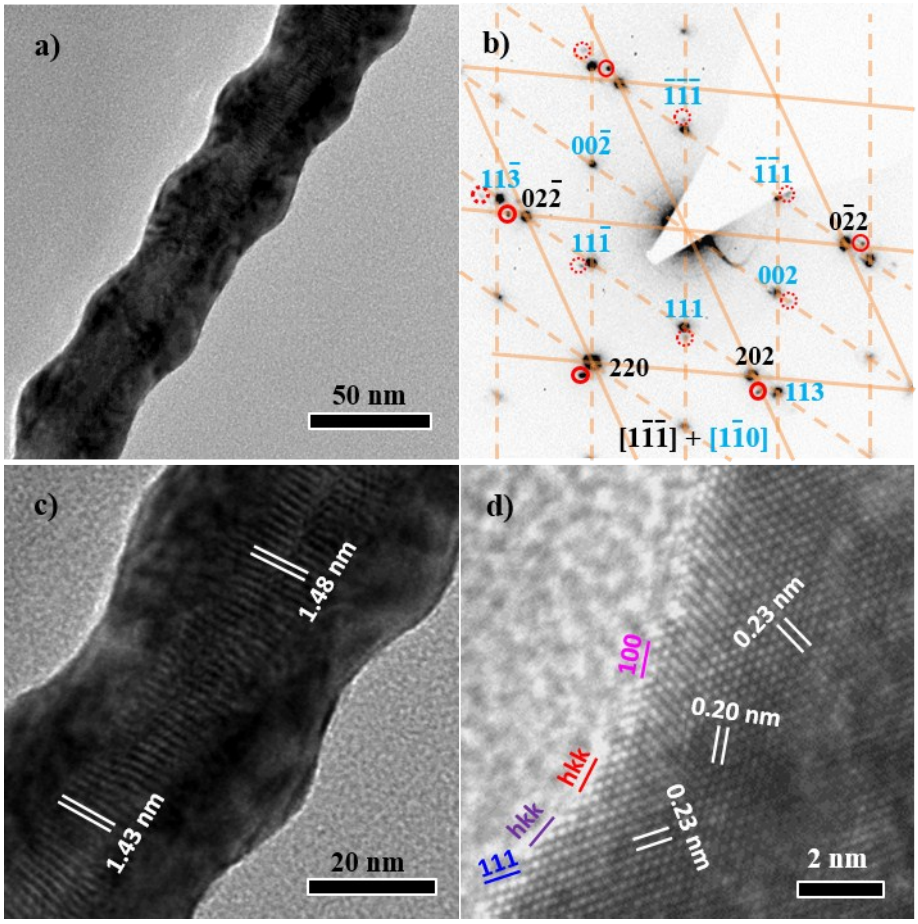

Fig. S11. The structure features of an individual wavy Cu@CuAu nanostructure. a) Low magnification TEM image of a part of the wavy Cu@CuAu nanostructure and b) corresponding SAED patterns; c) a magnified TEM image showing the Moiré fringes in the core region and d) HRTEM image recorded from the edge area.

Figure S11a and S11b show the TEM image and corresponding SAED pattern of a part of an individual wavy Cu@CuAu alloy nanostructure. The strong spots located on the cross points of the orange guides in the SAED patterns could be identified as two sets of spots and indexed

as the diffractions along $[1\bar{1}0]$ and $[1\bar{1}\bar{1}]$ zone axis of fcc structure, which were contributed by the five-fold twinned CuAu alloy structure of the shell. By investigating the SAED patterns carefully, other spots with weaker intensity can be found outside the most of the strong spots, some of them were marked by red circles. These weak spots marked by full circles and broken circles can be indexed as the diffractions along $[1\bar{1}\bar{1}]$ and $[1\bar{1}0]$ zone axis of *fcc* Cu structure, respectively, indicating that the five-fold twinned Cu core were still kept after the solvent treating. Figure S11c is the magnified TEM image of the wavy Cu@CuAu structure shown in Fig. S11a. The main feature of the image is the appearance of Moiré patterns in the core area, which were caused by the sandwich structure containing one layer Cu and two layers CuAu alloy of the Cu@CuAu nanocable structures. The d-spacing of CuAu alloy (220) could be calculated from the XRD patterns as 0.141 nm, the d-spacing of Cu (220) is known as 0.128 nm, the periodicity of the translational Moiré pattern can be calculated as D = 0.141*0.128/(0.141-0.128) = 1.4 nm, corresponding well with that measured from Fig. S11c. Fig. S11d is the high resolution TEM (HRTEM) image recorded from the edge area of Figure S5c, where ordered two dimensional lattices can be easily observed in the HRTEM images. The measured lattice spacing of 0.20 nm and 0.23 nm matches well with the CuAu alloy structure. And it can be deduced from the HRTEM image that the exposed surface of the wavy nanowires are consisted of complex high index facets.

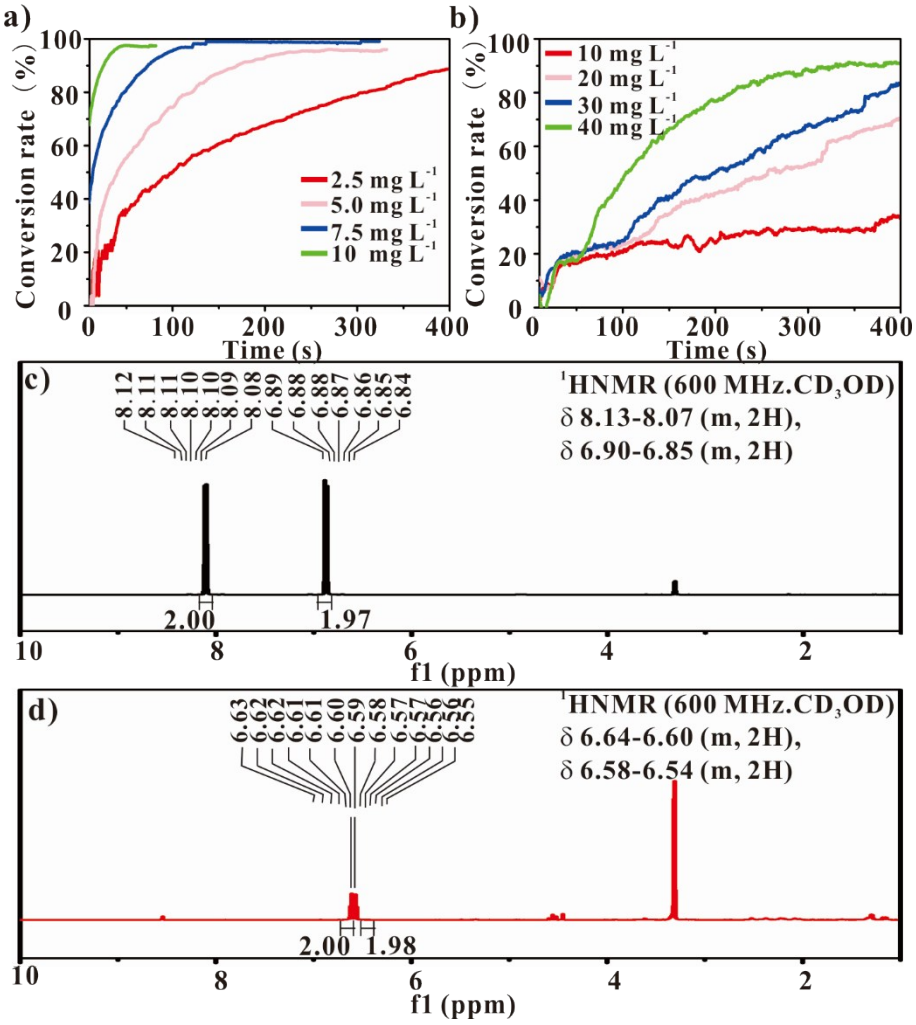

Fig. S12. The curves of the conversion rate of p-nitrophenol with a) wavy Cu@CuAu nanocables and b) the straight Cu@CuAu nanocable. HNMR spectrums of c) p-nitrophenol and d) the final products.

The time-depend curves of the conversion rate of p-nitrophenol indicated that the catalytic ability of the wavy Cu@CuAu nanocables is much stronger than the straight one. The conversion rate can reach 100% for 130 s at the concentration of only 7.5 mg·L^{-1} for the wavy Cu@CuAu nanocable catalysts. And the HNMR spectrums of the final products showed that the main product was p-aminophenol. While for the straight Cu@CuAu nanocable catalysts, the conversion rate can just reach to 90% at the concentration of 40 mg·L^{-1} for 400 s.

Q-SC potentials

The Q-SC potentials were developed by Goddard *et al.* to describe nine types of face-centered cubic metals (Al, Ni, Cu, Rh, Pd, Ag, Ir, Pt and Au).[1] The Q-SC parameters are optimized to describe the lattice parameter, cohesive energy, bulk modulus, elastic constant, phonon dispersion, vacancy formation energy, and surface energy. These potentials were tested by calculating the equation of states, thermal expansion and specific heat, and generally good agreement was found with all the properties. Meanwhile, the melting points of pure Cu and Au can be well reproduced by using these potentials. The obtained melting temperatures are consistence with the experimental results very well.[2] Therefore, we believe that the Q-SC potentials are appropriate and reliable for describing the properties of systems here.

According to the framework of the Q-SC potentials, the total energy for a system of atoms can be written as

$$U = \sum_i U_i = \sum_i \varepsilon \left[\frac{1}{2} \sum_{j \neq i} V(R_{ij}) - c\sqrt{\rho_i} \right], \qquad (2)$$

in which $V(R_{ij})$ is a pair interaction function defined by the following equation

$$V(R_{ij}) = \left(\frac{a}{R_{ij}} \right)^n, \qquad (3)$$

accounting for the repulsion between the *i* and *j* atomic cores; ρ_i is a local electron density accounting for cohesion associated with atom *i* defined by

$$\rho_i = \sum_{j \neq i} \left(\frac{a}{R_{ij}} \right)^m . \qquad (4)$$

In equations (2)-(4), R_{ij} is the distance between atoms *i* and *j*; *a* is a length parameter scaling all spacings (leading to dimensionless *V* and ρ); *c* is a dimensionless parameter scaling the attractive terms; ε sets the overall energy scale; *n* and *m* are integer parameters such that *n*

> m. Given the exponents (n, m), c is determined by the equilibrium lattice parameter, and ε is determined by the total cohesive energy. The model parameters for Cu and Au are listed in Table S1. In order to describe the interatomic interaction among them, the geometric mean was used to obtain the energy parameter ε while the arithmetic mean was used for the remaining parameters.[3,4]

Table S1. Potential parameters used in atomistic simulations for Cu-Au core-shell nanocable.

element	n	m	ε (meV)	c	A(Å)
Cu	10	5	5.7921	84.843	3.6030
Au	11	8	7.8052	53.581	4.0651

Density functional theory (DFT) calculation

In order to illustrate that the Cu atom can be extracted by the newly-formed Cu-amine complex, the correlative reactive potentials have been approximately estimated by DFT calculations. Since the binding energy of copper dimer Cu_2 is 46.4 kcal/mol, the relatively weak interaction between Cu atom and amine compound cannot extract Cu atoms.[5] According to the present experimental fact, the oxidation process of Cu atom is considered here. Combined the Table S2 and the equation $\Delta G=-nFE$, the free energy for the oxidation process is 25.9 kcal/mol. Furthermore, the copper atom is hexa-coordinated in *fcc* copper, indicating the surface copper atom is directly linked to five copper atoms and one ligand molecule, and thus the extraction reaction direction also depends on the bonding energies of Cu(II) – Cu(0) and Cu(II) – amine. Here a simple Cu(II)-Cu(0) model was constructed (Fig. S13), and the predicted bonding energy of Cu(II) – Cu(0) is 13.9 kcal/mol by B3LYP/6-311+G(d,p). We note that the bonding energies of Cu(II)-H_2O and Cu(II)-Lys (Lys = $NH_2(CH_2)_3CH_3$) in the octahedral configuration are 62.3 and 99.6 kcal/mol, respectively,[6] and Cu(II)-Lys bonding interactions are much stronger than Cu(II)-Cu(0), Cu(II)-H_2O, and Cu(0)-amine. The

thermodynamic data indicates that only the Cu(II)-Lys complex could be form to keep the oxidated copper ion away from the surface of Cu-Au alloy.

Table S2 Electrochemical potential of some electrode reactions

Electrode reaction	Normal potential (V)
$H_2O + O_2 + 4e^- = 4OH^-$	0.40
$Cu^{2+} + 2e^- = Cu$	0.34
$2Cu + H_2O + O_2 = 2Cu^{2+} + 4OH^-$	- 0.28

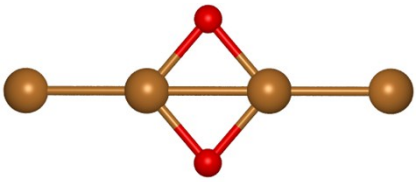

Fig. S13. The optimized structure of the simple Cu(II)-Cu(0) model.

References

1 T. Cagin, K. Kimura, Y. Qi, H. Li, H. Ikeda, W. L. Johnson and W. A. Goddard, *Mater. Res. Soc. Symp. Proc.,* 1999, **554**, 43-48.

2 F. Taherkhani, H. Akbarzadeh, M. Feyzi and H. R. Rafiee, *J. Nanopart. Res.,* 2015, **17**, 29.

3 S. K. R. S. Sankaranarayanan, V. R. Bhethanabotla and B. Joseph, *Phys. Rev. B,* 2005, **71**, 195415

4 H. Ikeda, Y. Qi, T. Cagin, K. Samwer, W. L. Johnson and W. A Goddard III, *Phys. Rev. Lett.,* 1999, **82**, 2900-2903.

5 J. L.Wang, G. H. Wang and J. J. Zhao, *Chem. Phys. Lett.*, 2003, **380**, 716–720.

6 L. Rulíšek and Z. Havlas, *J. Am. Chem. Soc.*, 2000, **122**, 10428–10439.